PLOS One

RESEARCH ARTICLE

Model predictive control based MLP-ANN to enhance tracking response with energy saving of EV drive cycles using five-phase IPMSM

Ahmed M. Hassan[1,2*], **Hamada Esmaiel**[3], **Mohammed M. Alammar**[3], **Mohamed Eladly Metwally**[2]

1 Department of Electrical Power and Machines Engineering, Faculty of Engineering, Benha University, Cairo, Egypt, **2** Department of Electrical Power and Machines Engineering, Higher Institute of Engineering (HIE), El-Shorouk Academy, El-Shorouk City, Egypt, **3** Electrical Engineering Department, College of Engineering, King Khalid University, Abha, Saudi Arabia

* ahmed.hassanin@feng.bu.edu.eg

OPEN ACCESS

Citation: Hassan AM, Esmaiel H, Alammar MM, Metwally ME (2026) Model predictive control based MLP-ANN to enhance tracking response with energy saving of EV drive cycles using five-phase IPMSM. PLoS One 21(2): e0340199. https://doi.org/10.1371/journal.pone.0340199

Editor: Mohamed Gamal Hussien, Tanta University Faculty of Engineering, EGYPT

Received: October 17, 2025

Accepted: December 16, 2025

Published: February 5, 2026

Data availability statement: All relevant data are within the paper and its Supporting Information files.

Funding: The authors (H.E) extend their appreciation to the Deanship of Research and Graduate Studies at King Khalid University for funding this work through Large Research

Abstract

Speed tracking control (STC) and energy saving of an electric vehicle (EV) play a crucial role in the stability and effectiveness of the operating performance of an EV drive system (EVDS). This paper proposes a novel STC and energy saving methodology for an EVDS that is tested by the European drive cycle (ECE-15) and customized inspection and maintenance drive cycle (custom IM240). The EVDS adopted the 5-ph interior permanent magnet synchronous motor (IPMSM) due to its benefits like high efficiency, compact size, low noise, reliability, reduced torque ripples, increased power density, and improved fault tolerance. A multilayer perceptron (MLP) - artificial neural network (ANN) is utilized to tune the PI controller online in the drive system (DS). The gating pulses of the 5-phase voltage source inverter (VSI) are accurately generated using an MPC based on a desired cost function to reduce current harmonics and thus torque ripples. A comparative study between the online tuning using the MLP-ANN and offline tuning using the transit search optimization (TSO) technique is presented. The process of comparison includes the percentage overshoot, mean square error (MSE), integral absolute error (IAE), and percentage energy saving. The result of the comparison proves the effectiveness of the proposed control methodology that gives superior speed tracking performance of the EVDS and attains energy saving. The attained energy saving across a long period results in cost reduction of charging the batteries and increasing their lifetime.

1 Introduction

Recently, air pollution reduction has received a lot of attention from the global community. Electric vehicles play an important role in the reduction of air pollution due to the absence of carbon emissions compared with traditional fuel vehicles [1,2]. To

Project under grant number RGP2/301/46. No additional external funding was received for this study. The funders had no role in study design, data collection and analysis, decision to publish, or preparation of the manuscript.

Competing interests: The authors have declared that no competing interests exist.

enhance the performance of the EV, a highly efficient drive system, effective speed tracking control, and energy-saving methodology should be introduced. The core of the EV drive system (EVDS) is the traction motor. There are several motors used in the EVDSs. The most used type is the IPMSM due to its benefits [2,3]. These benefits encompass excellent performance, low losses, compact size, etc. [2,4,5]. Because of their inherent benefits, multiphase motor drive systems (DSs) are becoming a promising alternative to 3-phase motor DSs. These benefits include reduced torque ripples and improved fault tolerance [6,7]. MPC is gaining prominence as a control method for DSs, showcasing exceptional performance and optimization [8].

The STC of an EV plays a vital role in the stability and effectiveness of the operating performance of the EV. Consequently, improving the speed response of an EV is considered to be an important subject. To the knowledge of the authors of this paper, there are no published papers that have studied the STC for an EV drive system utilizing a 5-phase IMPSM, MPC, and ANN online tuning to be driven according to different drive cycles. The analysis focuses on improving the speed tracking response that gives lower values of MSE, IAE, and speed overshoots across the whole operating period.

Literature survey of control methods regarding the adopted drive system is explored as follows:

Reference [9] introduced a sensorless control technique utilizing the 3rd harmonic space for a 5-ph PMSM. A direct torque MPC method for a five-phase PMSM was presented in [10]. In reference [11], a model predictive torque control (MPTC) technique was introduced for a 5-phase PMSM. Furthermore, reference [12] introduced an MPTC method that incorporates additional weighting factors to effectively reduce current harmonics and torque ripple. Reference [13] introduced a model-free predictive current control approach that leverages an ultra-local model and motor outputs for 5-phase PMSM DSs. Additionally, reference [14] proposed an MPCC approach for a five-phase PMPSM that employs voltage vector pre-selection.

Reference [15] evaluated different optimization methods to identify the best PI controller gains for a 3-phase PMSM DS. Reference [16] introduced an NN-based MPC method for regulating the speed of a 3-phase PMSM. Likewise, reference [17] introduced a control method using a BP ANN for a 3-phase PMSM. Reference [18] presented sensorless control of a PMSM by employing an adaptive speed observer (ASO). References [19–21] introduced a control method for a 3-phase PMSM, using an MPC-based ANN. Reference [22] introduced an MPC methodology for a 3-phase PMSM that employs dual-vector-based PSO.

Reference [23] introduced a deep reinforcement learning (DRL) methodology for controlling the speed of a 3-phase PMSM DS. This DRL control notably enhanced system performance, particularly in scenarios involving load variations. Reference [24] introduced DRL-based MPC to boost the efficiency of EVs. Reference [25] proposed a control methodology for a 3-phase PMSM using several optimization techniques and RL. Reference [26] suggested an RL control for a 3-phase PMSM, based on the twin delay deep deterministic (TD3) approach. Reference [27] compared the traditional PID method and an RL to control a PMSM, employing vector control (VC).

Reference [28] presented a combination of a hybrid adaptive nonlinear control (HANC) and a deadbeat observer (DO) to enhance the efficiency of a 3-phase PMSM, accommodating changes in load conditions and motor parameters. An adaptive fuzzy proportional-integral (AFPI) control scheme for a 3-phase PMSM was introduced in [29]. Reference [30] proposed an adaptive extended state observer to address peak issues and compensate for mismatched disturbances in a non-cascade-controlled PMSM. The impact of different hybrid EV powertrain options, including fuel cells, batteries, and supercapacitors, on component efficiency was investigated in [31]. Reference [32] introduced an adaptive speed control method utilizing a recurrent Elman neural network (RENN) to ensure good performance ST regardless of system uncertainties in the sensorless PMSM servo drive. A fractional order PID (FOPID) controller based on an adaptive neuro-fuzzy inference system for EV ST, utilizing a DC motor, was introduced in [33]. The performance, energy consumption, and robustness of the controller were evaluated using the New European Driving Cycle (NEDC) test. Reference [34] developed a simulation model for EV traction applications using a model-based design approach. The study incorporated a 3-phase IPMSM. A control algorithm for 3-phase PMSM-based EVs, incorporating the advantages of conventional proportional resonance (PR) and PI controllers, was introduced in Reference [35]. Reference [36] provided modeling and a comparative dynamic analysis of an FOC three-phase PMSM torque drive, utilizing both a hysteresis current controller and a PWM-operated current controller for energy-efficient EVs. Various EV batteries performance was evaluated in Reference [37] using different drive cycles. Reference [38] introduced a control methodology for the DS of an EV's PMSM. It utilized a robust non-linear MPC in a cascaded structure, combined with SVPWM. A drive control methodology for a three-phase PMSM powered by a multi-level inverter for EV applications was presented in [39]. The study also involved designing an active damping and current controller to deliver a rapid and precise torque response to the induced torsional moments. A machine learning (ML) based controller for a 3-phase PMSM DS was presented in [40]. Reference [41] presented an RL control methodology based on the TD3 technique for tuning cascaded PI controllers in a DS utilizing 5-phase PMSM and MPC.

In this research, a new speed tracking control and energy saving methodology for the EV drive system is proposed and tested by ECE-15 and IM240 drive cycles. The adopted drive system is composed of an EV, 5-phase VSI, 5-phase IPMSM, PI controller, and MPC. The PI controller is tuned using an MLP-ANN online tuning to generate the reference torque signal. This overcomes any load variation compared with offline tuning. The load variation is represented by the test drive cycles. The reference torque signal is utilized to obtain the reference direct and quadrature current to verify the operation of the 5-ph IMPSM at MTPA to attain high efficiency and thus low losses. The MPC is used in the drive system to generate the gating pulses for the 5-phase VSI according to the desired reference direct and quadrature currents. To validate the presented control method, simulation results are generated using MATLAB Simulink. To indicate the effectiveness of the proposed control methodology, several results are obtained when an offline tuning for the PI controller is compared with those obtained when the ANN online tuning is used. The process of comparison includes the percentage overshoot, MSE, IAE, and energy saving performance. In the offline tuning, the PI controller gains are obtained using a metaheuristic optimization technique called Transit Search.

The main contributions of this paper can be summarized as follows:

- A methodology of control for a high-performance EV drive system is proposed and verified using two drive cycles to enhance the speed tracking response and to attain energy saving.
- A comparative analysis is carried out between the presented methodology of control, which is based on MLP-ANN online tuning, and the conventional offline tuning method to prove the effectiveness of the proposed methodology compared with the conventional method.
- The presented control methodology can be considered as a saving energy method.
- A MATLAB SIMULINK is carried out for the EVDS under consideration to validate the presented control method.

The structure of the remaining sections of this paper is as follows: Section 2 introduces the EVDS model. Section 3 introduces an explanation of the MPC. Section 4 covers the MLP-ANN online tuning. Section 5 explains the transit search optimization technique. Section 6 explores the results. Section 7 presents the summary of the findings.

2 Modeling of the EV drive system

In the following subsections, each part of the EVDS shown in Fig 1 will be introduced.

2.1 Drive cycle model

The drive cycles are modeled in terms of their speed-time graph. The adopted drive cycles in this paper are the European drive cycle (ECE-15), Fig 2 [31], and the customized inspection and maintenance drive cycle (IM240), Fig 3 [42]. Table 1 indicates the characteristics of the two drive cycles.

2.2 EV model. The input of the vehicle model is the velocity obtained from the drive cycle. The model outputs are the required vehicle torque and the required motor speed. The vehicle torque can be obtained by calculating the total force. The total force is the resultant of the forces affecting the vehicle. These forces are aerodynamic force, rolling force, gradient force, and inertia force, as shown in Fig 4.

The aerodynamic force, *Fairodynamic*, can be expressed in the following formula [2,34,39]:

$$F_{airodynamic} = \frac{1}{2}\rho_a C_{ad} A_{fa} (V_v + V_{wind})^2 \tag{1}$$

Where *ρa* is the air density in kg/m3, *Cad* is the aerodynamic drag coefficient, *Afa* is the vehicle frontal area in m2, *Vv* is the vehicle velocity in m/s, and *Vwind* is the wind speed in m/s. The tyre rolling force, *Frolling*, takes the following form [2,34,39]:

$$F_{rolling} = m_v g_a C_{rr} \cos\theta_i \tag{2}$$

Where *mv* is the vehicle mass in kg, ga is the gravitational acceleration, *Crr* is the tyre rolling resistance coefficient, and *θi* is the vehicle inclination angle in degrees. The following formula indicates the gradient force, *Fgradient* [2,34,39]:

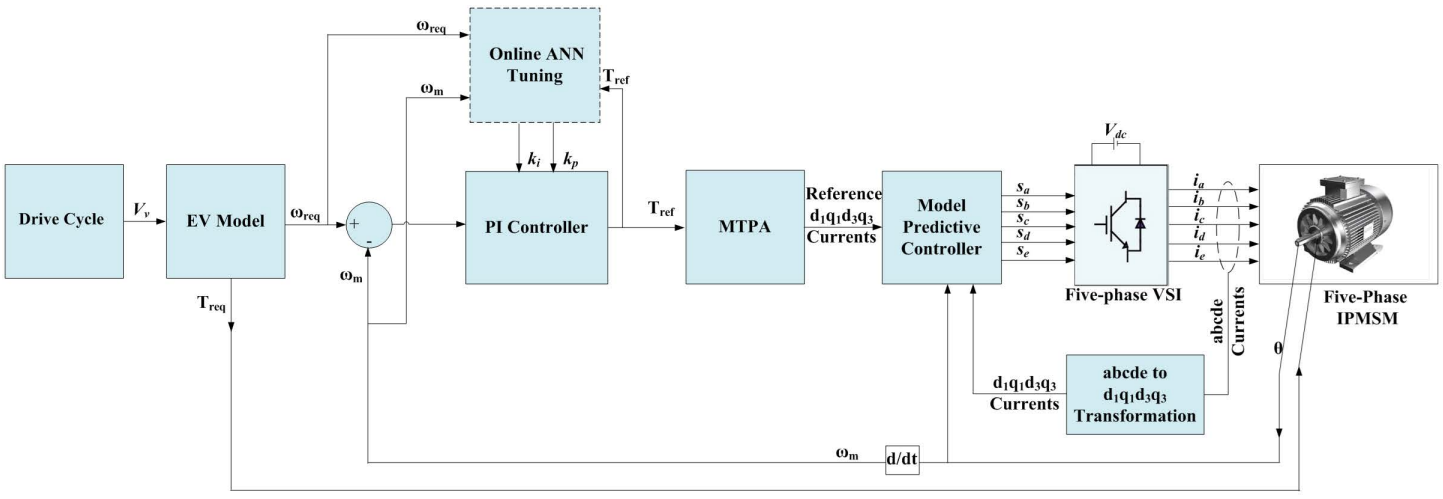

Fig 1. EV drive system under consideration.

https://doi.org/10.1371/journal.pone.0340199.g001

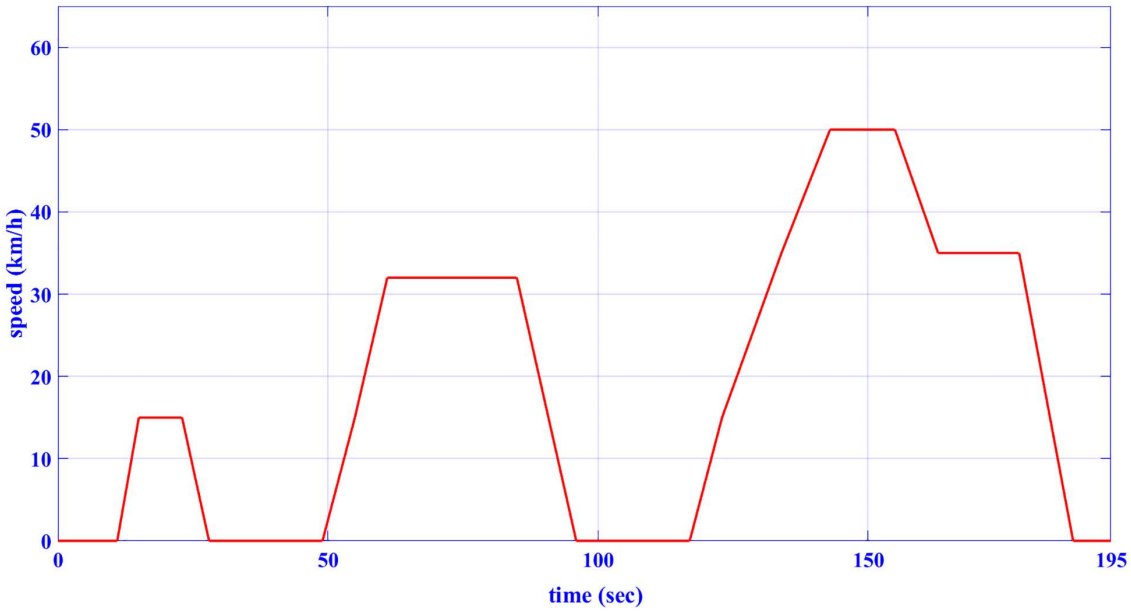

Fig 2. ECE-15 drive cycle [31].

https://doi.org/10.1371/journal.pone.0340199.g002

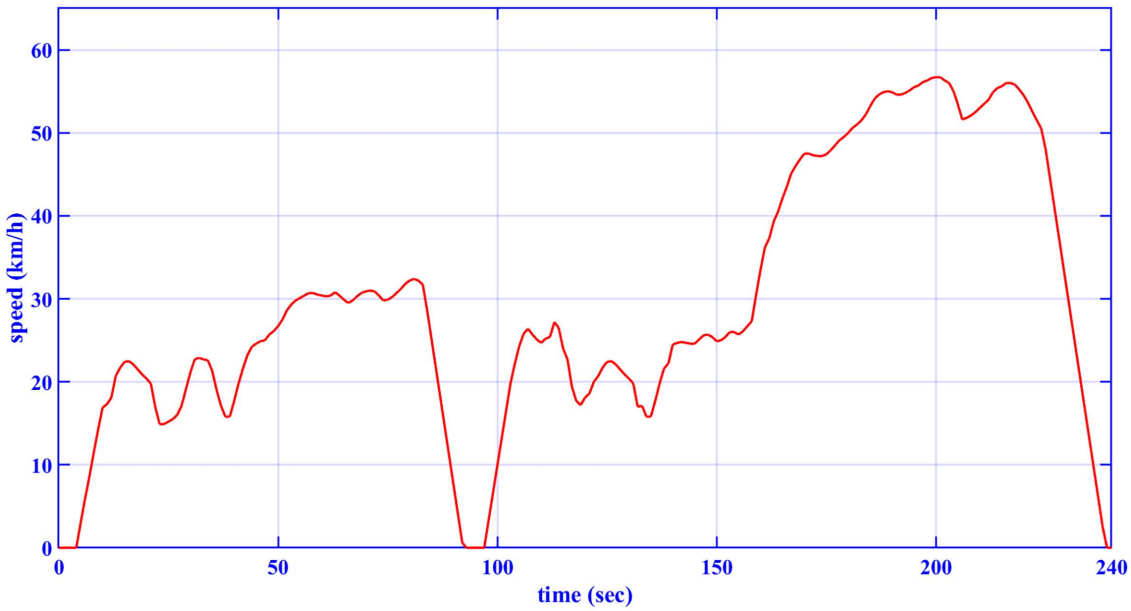

Fig 3. IM240 drive cycle [42].

https://doi.org/10.1371/journal.pone.0340199.g003

$$F_{gradient} = m_v g_a \sin\theta_i \tag{3}$$

The inertia force, *Finertia*, can be expressed in the following formula [2,34,39]:

Table 1. Characteristics of the drive cycles.

Features	ECE-15	Custom IM240
Distance	0.9941 km	3.1 km
Total time	195 s	240 s
Average speed (incl. stops)	18.35 km/h	29.4 km/h
Maximum speed	50 km/h	57.6 km/h

https://doi.org/10.1371/journal.pone.0340199.t001

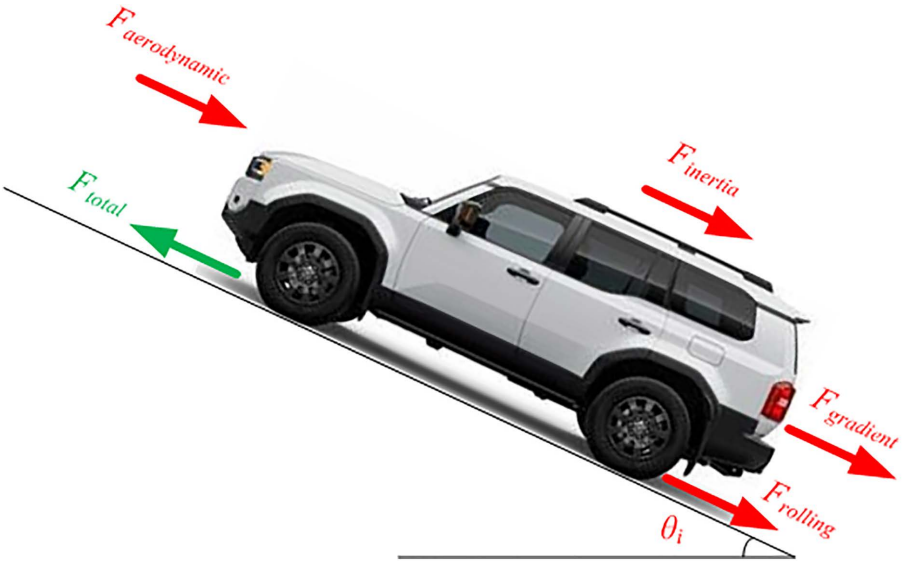

Fig 4. Forces affecting the total force of an electric vehicle.

https://doi.org/10.1371/journal.pone.0340199.g004

$$F_{inertia} = m_v a_v \tag{4}$$

Where *av* is the vehicle acceleration. Thus, the total vehicle force can be obtained from the following formula [2,34,39]:

$$F_{total} = F_{aerodynamic} + F_{rolling} + F_{gradient} + F_{inertia} \tag{5}$$

Consequently, the required motor torque can be obtained from [2,34,39]:

$$T_{req} = F_{total} R_{wheel} / G_R \tag{6}$$

Where *Rwheel* is the vehicle wheel radius, and *GR* is the gear ratio. Also, the motor required speed can be obtained from [2,34,39]:

$$\omega_{req} = G_R V_v / R_{wheel} \tag{7}$$

The EV required power can thus be obtained from:

$$P_{req} = T_{req} \omega_{req} \tag{8}$$

In addition to this, the required energy can be expressed as:

$$E_{req} = \int P_{req} dt \tag{9}$$

2.3 5-Phase VSI model. The VSI is represented through the voltages (*va* to *ve*), which are influenced by switching functions of the VSI [10,41].

$$\begin{bmatrix} v_a \\ v_b \\ v_c \\ v_d \\ v_e \end{bmatrix} = \frac{V_{dc}}{5} \begin{bmatrix} 4 & -1 & -1 & -1 & -1 \\ -1 & 4 & -1 & -1 & -1 \\ -1 & -1 & 4 & -1 & -1 \\ -1 & -1 & -1 & 4 & -1 \\ -1 & -1 & -1 & -1 & 4 \end{bmatrix} . \begin{bmatrix} s_a \\ s_b \\ s_c \\ s_d \\ s_e \end{bmatrix} \tag{10}$$

In Eq. (10), Vdc denotes the battery voltage. The switching functions, labeled as Sa to Se, indicate the different VSI switching states. A switching function takes the value of one when the upper switch in a leg is ON, and zero when the lower switch of this leg is OFF. There are 32 switching states. The MPC provides the optimal switching state that gives a minimized cost function. According to the selected state from the 32 states, gate pulses are provided to ten switches of the VSI.

2.4 5-phase IPMSM model. The 5-phase IPMSM is characterized by the aiding of the direct-quadrature analysis in a synchronously rotating reference frame. The transformations from voltage ABCDE to DQ are detailed in [10,41,43].

$$\begin{bmatrix} v_{d1} \\ v_{q1} \\ v_{d3} \\ v_{q3} \\ v_0 \end{bmatrix} = \frac{2}{5} \begin{bmatrix} \cos\theta & \cos(\theta-\alpha) & \cos(\theta-2\alpha) & \cos(\theta+2\alpha) & \cos(\theta+\alpha) \\ -\sin\theta & -\sin(\theta-\alpha) & -\sin(\theta-\alpha) & -\sin(\theta+2\alpha) & -\sin(\theta+\alpha) \\ \cos 3\theta & \cos 3(\theta-\alpha) & \cos 3(\theta-2\alpha) & \cos 3(\theta+2\alpha) & \cos 3(\theta+\alpha) \\ -\sin 3\theta & -\sin 3(\theta-\alpha) & -\sin 3(\theta-2\alpha) & -\sin 3(\theta+2\alpha) & -\sin 3(\theta+\alpha) \\ \frac{1}{\sqrt{2}} & \frac{1}{\sqrt{2}} & \frac{1}{\sqrt{2}} & \frac{1}{\sqrt{2}} & \frac{1}{\sqrt{2}} \end{bmatrix} . \begin{bmatrix} v_a \\ v_b \\ v_c \\ v_d \\ v_e \end{bmatrix} \tag{11}$$

Where the value of α is 2π/5, *vd1* and *vq1* are the DQ fundamental stator voltages, *vd3* and *vq3* are the 3rd harmonic DQ stator voltages, and θ represents the rotor position angle.

To transform from the DQ to the ABCDE quantities, the following equation can be used [10,41]:

$$\begin{bmatrix} i_{as} \\ i_{bs} \\ i_{cs} \\ i_{ds} \\ i_{es} \end{bmatrix} = \begin{bmatrix} \cos\theta & -\sin\theta & \cos 3\theta & -\sin 3\theta & \frac{1}{\sqrt{2}} \\ \cos(\theta-\alpha) & -\sin(\theta-\alpha) & \cos 3(\theta-\alpha) & -\sin 3(\theta-\alpha) & \frac{1}{\sqrt{2}} \\ \cos(\theta-2\alpha) & -\sin(\theta-2\alpha) & \cos 3(\theta-2\alpha) & -\sin 3(\theta-2\alpha) & \frac{1}{\sqrt{2}} \\ \cos(\theta+2\alpha) & -\sin(\theta+2\alpha) & \cos 3(\theta+2\alpha) & -\sin 3(\theta+2\alpha) & \frac{1}{\sqrt{2}} \\ \cos(\theta+\alpha) & -\sin(\theta+\alpha) & \cos 3(\theta+\alpha) & -\sin 3(\theta+\alpha) & \frac{1}{\sqrt{2}} \end{bmatrix} . \begin{bmatrix} i_{d1} \\ i_{q1} \\ i_{d3} \\ i_{q3} \\ i_0 \end{bmatrix} \tag{12}$$

Where *id1* and *iq1* are the DQ fundamental stator currents, and *id3* and *iq3* are the DQ 3rd harmonic stator currents.

The differential equation of the 5-phase IPMSM can be expressed as follows [41]:

$$D[I] = [LL][V] - [LR].[I] - \omega[L\lambda].[I] + \omega[LG].[I] \tag{13}$$

Where D is the differentiator d/dt, $[I] = [\ i_{d1} \quad i_{q1} \quad i_{d3} \quad i_{q3}\ ]^T$, $[V] = [\ v_{d1} \quad v_{q1} \quad v_{d3} \quad v_{q3}\ ]^T$,

$$[LL] = \begin{bmatrix} \frac{-L_{d3}}{L_{m13}^2 - L_{d1}L_{d3}} & 0 & \frac{L_{m13}}{L_{m13}^2 - L_{d1}L_{d3}} & 0 \\ 0 & \frac{-L_{q3}}{L_{m13}^2 - L_{q1}L_{q3}} & 0 & \frac{L_{m13}}{L_{m13}^2 - L_{q1}L_{q3}} \\ \frac{L_{m13}}{L_{m13}^2 - L_{d1}L_{d3}} & 0 & \frac{-L_{d1}}{L_{m13}^2 - L_{d1}L_{d3}} & 0 \\ 0 & \frac{L_{m13}}{L_{m13}^2 - L_{q1}L_{q3}} & 0 & \frac{-L_{q1}}{L_{m13}^2 - L_{q1}L_{q3}} \end{bmatrix}$$

$$[LR] = \begin{bmatrix} \frac{-L_{d3}R_s}{L_{m13}^2 - L_{d1}L_{d3}} & 0 & \frac{L_{m13}R_s}{L_{m13}^2 - L_{d1}L_{d3}} & 0 \\ 0 & \frac{-L_{q3}R_s}{L_{m13}^2 - L_{q1}L_{q3}} & 0 & \frac{L_{m13}R_s}{L_{m13}^2 - L_{q1}L_{q3}} \\ \frac{L_{m13}R_s}{L_{m13}^2 - L_{d1}L_{d3}} & 0 & \frac{-L_{d1}R_s}{L_{m13}^2 - L_{d1}L_{d3}} & 0 \\ 0 & \frac{L_{m13}R_s}{L_{m13}^2 - L_{q1}L_{q3}} & 0 & \frac{-L_{q1}R_s}{L_{m13}^2 - L_{q1}L_{q3}} \end{bmatrix}$$

$$[LG] = \begin{bmatrix} 0 & \frac{3L_{m13}^2 - L_{d3}L_{q1}}{L_{m13}^2 - L_{d1}L_{d3}} & 0 & \frac{3L_{m13}L_{q3} - L_{d3}L_{m13}}{L_{m13}^2 - L_{d1}L_{d3}} \\ \frac{L_{d1}L_{q3} - 3L_{m13}^2}{L_{m13}^2 - L_{q1}L_{q3}} & 0 & \frac{L_{m13}L_{q3} - 3L_{d3}L_{m13}}{L_{m13}^2 - L_{q1}L_{q3}} & 0 \\ 0 & \frac{L_{m13}L_{q1} - 3L_{d1}L_{m13}}{L_{m13}^2 - L_{d1}L_{d3}} & 0 & \frac{L_{m13}^2 - 3L_{d1}L_{q3}}{L_{m13}^2 - L_{d1}L_{d3}} \\ \frac{3L_{m13}L_{q1} - L_{d1}L_{m13}}{L_{m13}^2 - L_{q1}L_{q3}} & 0 & \frac{3L_{d3}L_{q1} - L_{m13}^2}{L_{m13}^2 - L_{q1}L_{q3}} & 0 \end{bmatrix}$$

$$[L\lambda] = \begin{bmatrix} 0 \\ \frac{3\lambda_{3m}L_{m13} - \lambda_{1m}L_{q3}}{L_{m13}^2 - L_{q1}L_{q3}} \\ 0 \\ \frac{\lambda_{1m}L_{m13} - 3\lambda_{3m}L_{q1}}{L_{m13}^2 - L_{q1}L_{q3}} \end{bmatrix}$$

Where *Rs* represents the per-phase resistance, ω denotes electrical angular speed, *Ld1* and *Lq1* represent the DQ fundamental self-inductances, *Ld3* and *Lq3* represent the DQ 3rd harmonic self-inductances, *Lm13* is the mutual inductance, and *λ1m*, *λ3m* are the PM fluxes for the fundamental and 3rd component.

The motor torque can be expressed as [10,41,43]:

$$T_e = \frac{5}{2}\frac{p}{2}[(L_{d1} - L_{q1})i_{d1}i_{q1} + 2L_{m13}(i_{d1}i_{q3} - i_{q1}i_{d3}) + 3(L_{d3} - L_{q3})i_{d3}i_{q3} + (\lambda_{1m}i_{q1} + 3\lambda_{3m}i_{q3})] \tag{14}$$

Where p is the number of poles.

The mechanical equation can be expressed as [41]:

$$D\omega_m = \frac{T_e - T_l(\omega_m)}{J} \tag{15}$$

where J is the inertia, and $T_l(\omega_m)$ is given by:

$$T_l(\omega_m) = T_L + T_{fw} \tag{16}$$

Where T_L is the load torque and T_{fw} is the friction and windage torque.

2.5 5-phase IPMSM MTPA operating model. To achieve maximum efficiency, the 5-phase IPMSM operates at MTPA. When Lm13 is neglected, the fundamental and third-harmonic DQ currents, that give MTPA, can be obtained from [41]:

$$i_{d1} = \frac{\lambda_{1m}}{2(L_{q1} - L_{d1})} - \sqrt{\frac{\lambda_{1m}^2}{4(L_{q1} - L_{d1})^2} + i_{q1}^2} \tag{17}$$

$$i_{q1} = \frac{T_{e1}}{\frac{5}{2}\frac{p}{2}[(L_{d1} - L_{q1})i_{d1} + \lambda_{1m}]} \tag{18}$$

Also, the 3rd harmonic direct and quadrature currents can be obtained from [41,44]:

$$i_{d3} = k\sqrt{i_{d1}^2 + i_{q1}^2}\,\sin\{3[\tan^{-1}(\frac{i_{d1}}{i_{q1}})]\} \tag{19}$$

$$i_{q3} = k\sqrt{i_{d1}^2 + i_{q1}^2}\,\cos\{3[\tan^{-1}(\frac{i_{d1}}{i_{q1}})]\} \tag{20}$$

3 Model predictive control technique

MPC is composed of a plant model and an optimizer. The main objective of MPC is the selection of the best arrangement of inputs for the system by forecasting its behavior in the future. The forecasts are generated by the plant model, which relies on past states to predict the next ones. At every sampling period, the optimizer utilizes the forecasted states and the required trajectory to solve the problem of optimization over the forecasting horizon, thus determining the optimized group of inputs for future executions.

To effectively achieve MPC, it is essential to discretize the 5-phase IPMSM model. Therefore, eqn. (13) is transformed into its discrete form as follows [41]:

$$[I(k+1)] = [I(k)] + T_s\{[LL][V] - [LR].[I(k)] - \omega[L\lambda].[I(k)] + \omega[LG].[I(k)]\} \tag{21}$$

Where Ts is the sampling period.

The main objective of the MPC is to minimize torque error. The torque error can be minimized by minimizing the DQ currents errors. Consequently, the cost function (CF) that minimizes the DQ currents errors can be written in the following form [41]:

$$C.F = [i_{d1r} - i_{d1}(k+1)]^2 + [i_{q1r} - i_{q1}(k+1)]^2 + [i_{d3r} - i_{d3}(k+1)]^2 + [i_{q3r} - i_{q3}(k+1)]^2 \tag{22}$$

Here, (*id1r*, *iq1r*, *id3r*, and *iq3r*) denote the reference DQ currents. They can be calculated with the aid of equations (17), (18), (19), and (20). The optimum 5-phase VSI switching functions are selected according to the lowest CF.

4 Proposed adaptive PI-ANN controller

The mathematical formulation of a conventional PI controller is expressed as follows:

$$u(t) = K_P e_t(t) + K_i \int e_t(t)\ dt \tag{23}$$

Here, K_P is the proportional gain and K_i is the integral gain. $e_t(t)$ represents the speed error signal, and $u(t)$ is the controller output. These PI parameters are typically set to constant values using methods such as Ziegler-Nichols' first tuning method [45].

ANN provides a data-driven approach to model system behavior through learning mechanisms based on error minimization criteria. In this study, a multi-layer perceptron (MLP) ANN was implemented in an offline mode for training. The MLP architecture consists of a single hidden layer with 20 neurons, as shown in Fig 5. The model of the MLP-ANN and its associated learning error criteria are represented as follows [45]:

$$\hat{y} = W_{out}^T \tanh\left(W_{in}^T X + b_{in}\right) + b_{out} \tag{24}$$

$$E = \frac{1}{2}\sum(e)^2 = \frac{1}{2}\sum(y - \hat{y})^2 \tag{25}$$

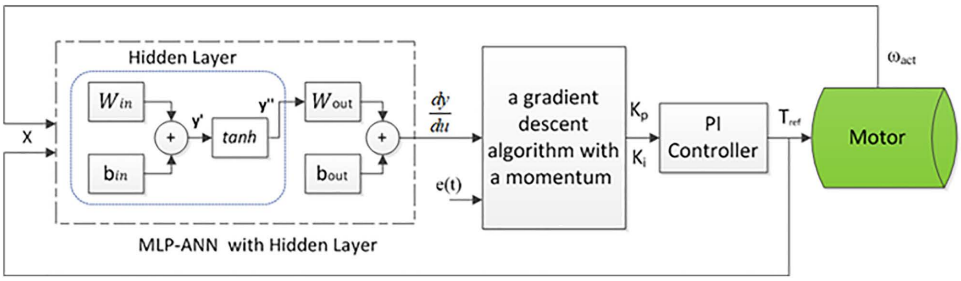

Fig 5. The proposed adaptive PI-ANN controller.

https://doi.org/10.1371/journal.pone.0340199.g005

Where X is the input vector, y is the actual output, $\hat{y}$ is the predicted output, e is the error signal, and E denotes MSE used as the CF. The terms W_{in}, W_{out}, b_{in}, and b_{out} represent the weights and biases of the ANN.

The proposed adaptive PI-ANN control strategy leverages the MLP-ANN model [45]. By utilizing the Jacobian matrix of the system, the K_P and K_i are updated in each iteration of the control loop. The block diagram of the suggested control algorithm is depicted in Fig 5. This approach incorporates the Jacobian matrix to compute the gradient vector, enabling the adjustment of the PI parameters using the chain rule of the backpropagation algorithm, as shown below:

$$\frac{dy}{du} \cong \frac{d\hat{y}}{du} = W_{in}^{T} W_{out}^{T} \frac{dy''}{dy'} \tag{26}$$

$$\frac{dE}{dK_{P,i}} = \frac{dE}{de}\frac{de}{d\hat{y}}\frac{d\hat{y}}{dX}\frac{dX}{du}\frac{du}{dK_{P,i}} \tag{27}$$

Here $\frac{dy}{du} \cong \frac{d\hat{y}}{du}$ represents the Jacobian matrix of the ANN, $\frac{dy''}{dy'} = 1 - tanch^2(y')$ is the differentiation of the function of activation, $\frac{dE}{dK_{P,i}}$ are the derivatives of the CF w.r.t the PI parameters, $\frac{dE}{de}$ is the derivative of the CF w.r.t the error, $\frac{de}{d\hat{y}}$ is determined as −1, $\frac{du}{dK_{P,i}}$ are the derivatives of the control signal $u(t)$ with respect to the PI parameters, $\frac{du}{dK_P} = e_t(t)$ and $\frac{du}{dK_i} = \int_0^{\infty} e_t(t)\ \mathrm{dt}$, and $e_t(t)$ is the closed-loop error signal.

To adaptively update the PI parameters, a gradient descent algorithm with a momentum term [45] is employed. This iterative update rule is given as follows:

$$K_{P,i}(n) = K_{P,i}(n-1) - \alpha VK_{P,i}(n) \tag{28}$$

$$VK_{P,i}(n) = \beta \nabla_{K_{P,i}}(n-1) + (1-\beta)\nabla_{K_{P,i}}(n) \tag{29}$$

In this equation, $K_{P,i}$ are the PI parameters, $\nabla_{K_{P,i}} = \frac{du}{dK_{P,i}}$ is the gradient, n is the iteration number, α is the learning rate, and β is the momentum coefficient. The flowchart for the suggested algorithm is shown in Fig 6.

5 Transit search optimization technique

A TSO algorithm [46] model is achieved for optimal tuning of the PI controller.

(5.1) Objective

The optimization objective concentrates on minimizing the speed error by tuning its controllers' gains. The controller contains two gains (proportional gain KP and the integral gain KI). The gains have a lower limit [0 0] and upper limit [100 100].

$$Target = min\ (error) \tag{30}$$

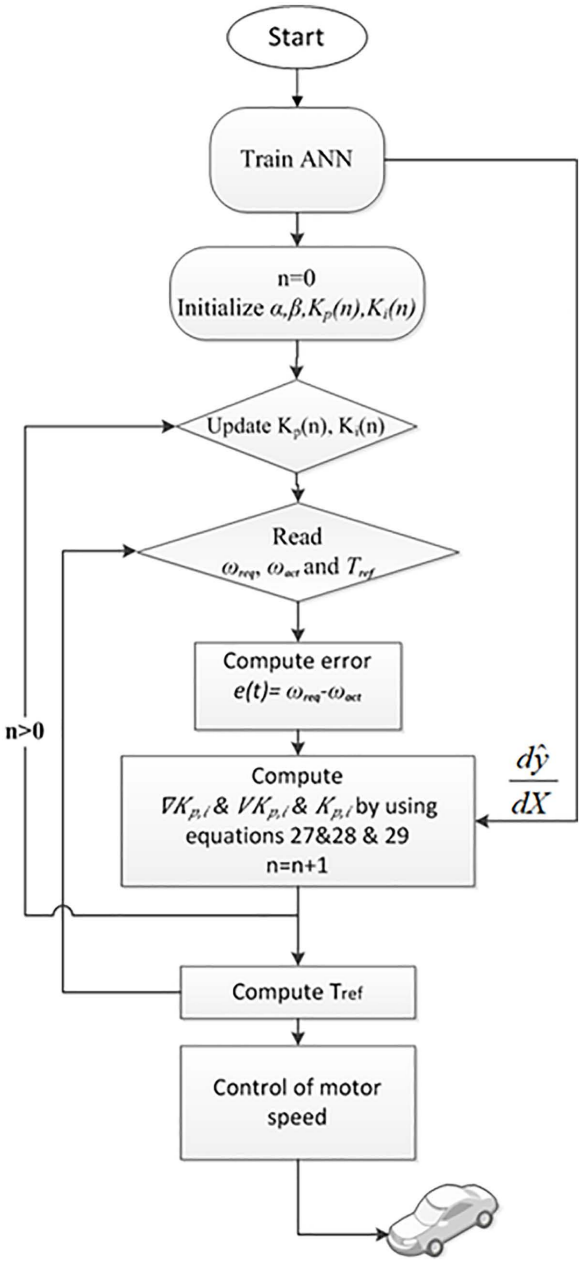

Fig 6. Flowchart Proposed Adaptive PI Control Algorithm.

https://doi.org/10.1371/journal.pone.0340199.g006

$$error = \int (\omega_{actual} - \omega_{ref})^2 dt$$

(5.2) Transit search algorithm

The flowchart of the TSO algorithm steps, which is used in this work, is shown in Fig 7. The optimization process is composed of five split phases in the TSO algorithm. First, Galaxy phase: executes for initialization by assigning a galaxy

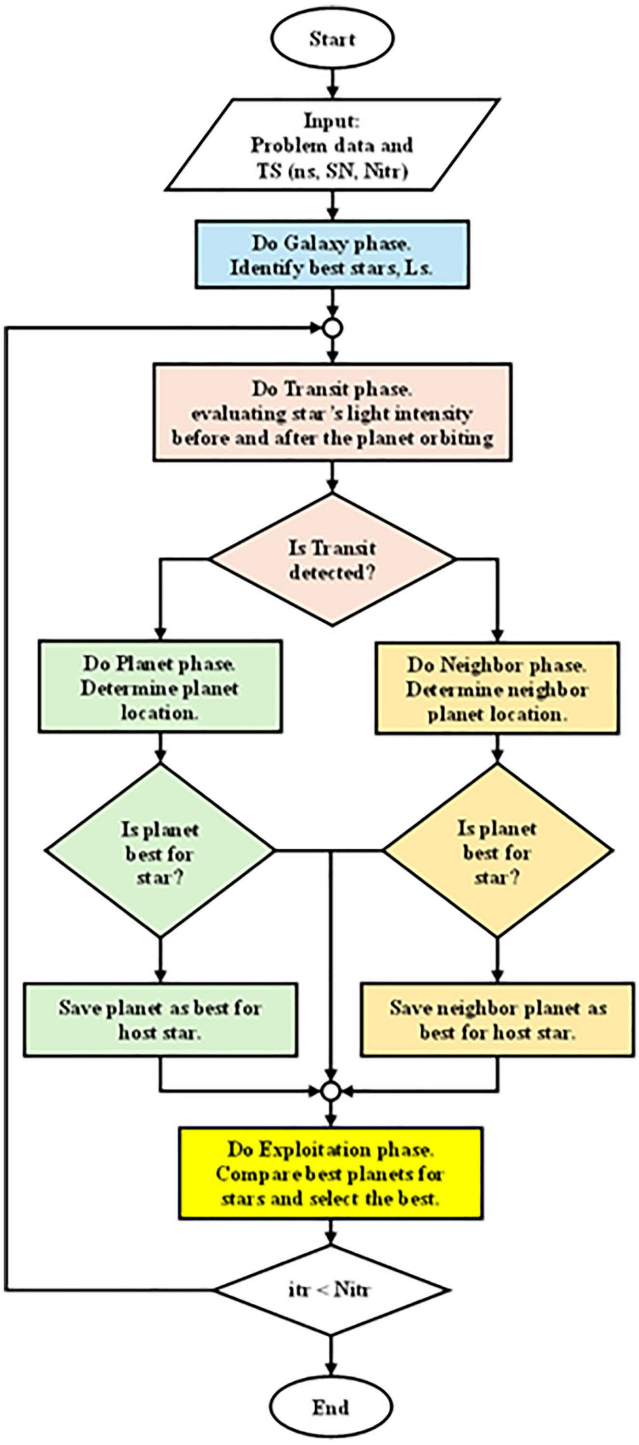

Fig 7. Flowchart of the TSO algorithm.

https://doi.org/10.1371/journal.pone.0340199.g007

center in a random way to determine a galaxy and its habitable zones and determine the proper position of the star. Second, the Transit phase starts by assessing the change in the star's intensity of light during the rotation of the planet. Third, Planet phase: when a planet transit is detected, the initial position of the specific planet is calculated. In every iteration, the planet identified with better fitness is marked. Fourth, Neighbor phase: executes when transit isn't detected by analyzing the neighboring planet and replacing the present planet in case it has better fitness. Finally, the phase of exploitation determines the best planet for every star by studying many scenarios of the imported existing knowledge from the previous phases.

6 Results

Several simulation results are obtained to ensure the validity of the presented control methodology for the EV drive system under consideration using the two test driving cycles, ECE-15 and custom IM240. The vehicle parameters are given in Table 2 [34]. The parameters of the motor are given in Table 3 [10]. The inclination angle, θi, is taken to be 25°. The offline tuning gains, kp and ki for the PI controller, are obtained at motor rated condition using Transit Search optimization (TSO) technique [46] and found to be 10.3486 and 25.0843, respectively.

Figs 8 and 9 show the reference and actual motor speeds for both drive cycles when the PI controller is tuned either offline using TSO or online using MLP-ANN. It can be noticed that there are many overshoots in the motor

Table 2. Electric vehicle parameters.

Parameter	Value
Kerb and passenger weight (mv), kg	158
Frontal area (Afa), m2	0.875
Wheel radius (Rwheel), m	0.23
Aerodynamic drag coefficient (Cad)	0.22
Gear ratio (GR)	3.1:1
Tyre rolling resistance coefficient (Crr)	0.03

https://doi.org/10.1371/journal.pone.0340199.t002

Table 3. 5-Table 4Table 5ph IPMSM parameters.

Parameter	Value
poles (p)	4 poles
Nominal power	12 kW
Nominal Speed	1800 rpm
Base speed	5400 rpm
Nominal Torque	63.662 Nm
Rs	0.389 Ω
Ld1	2.7 mH
Lq1	9.6 mH
Ld3	1.1 mH
Lq3	2 mH
Lm13	0 mH
λ1m	0.11 WbT
λ3m	0.0012 WbT
Motor moment of inertia	0.0036 kg.m2
Total moment of inertia	0.14 kg.m2
Connection	Star

https://doi.org/10.1371/journal.pone.0340199.t003

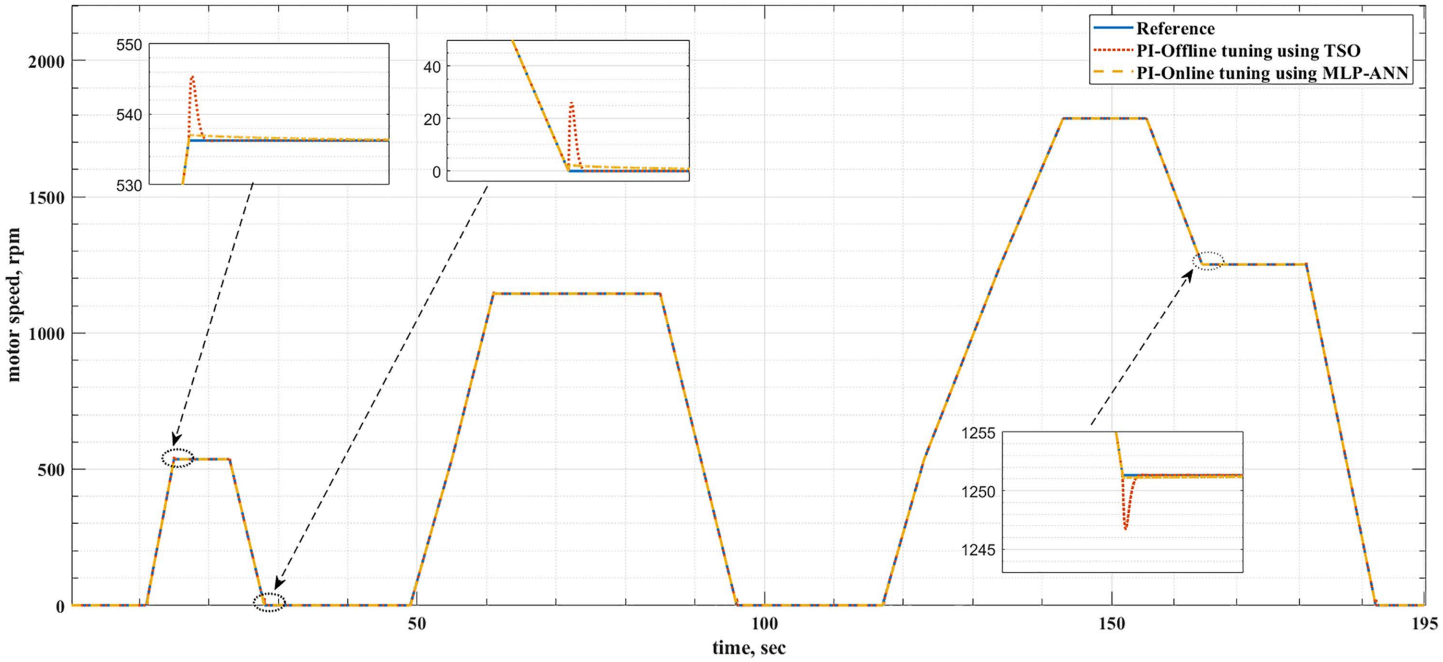

Fig 8. The reference and actual motor speeds for the ECE-15 drive cycle when offline and online PI tuning are used.

https://doi.org/10.1371/journal.pone.0340199.g008

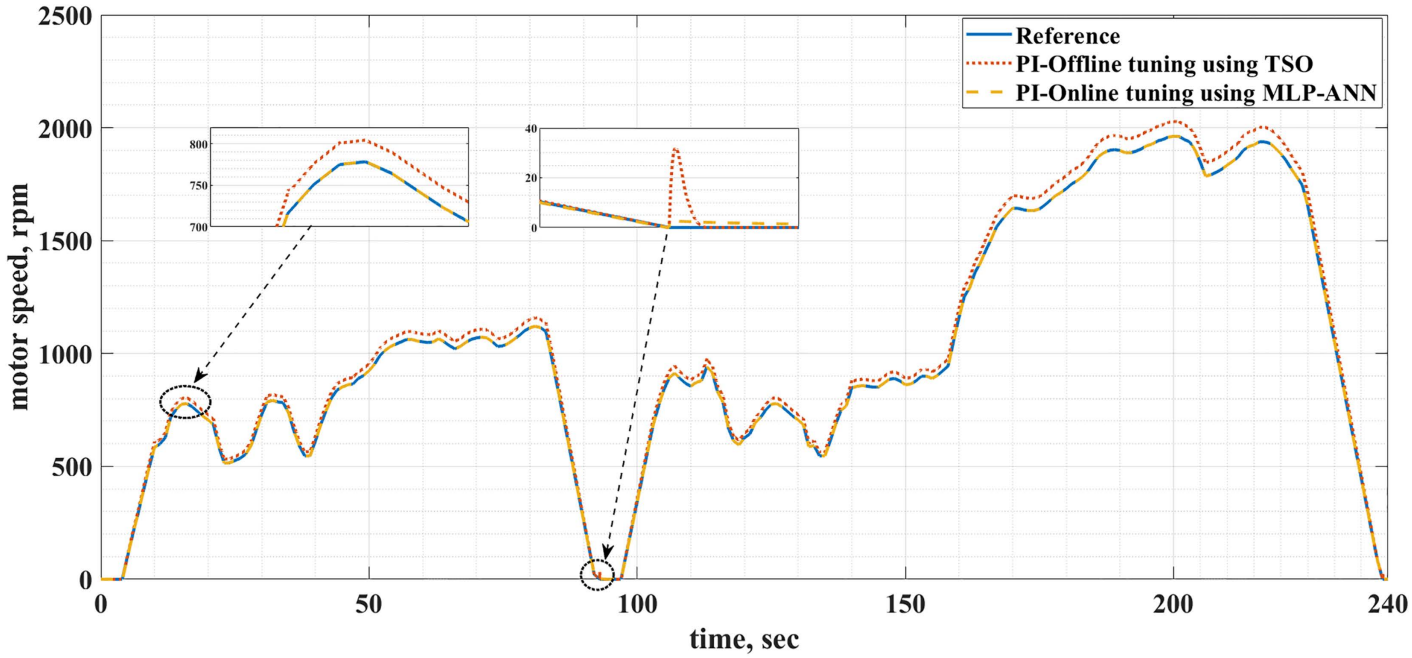

Fig 9. The reference and actual motor speeds for the custom IM240 drive cycle when offline and online PI tuning are used.

https://doi.org/10.1371/journal.pone.0340199.g009

speed when the offline tuning is used. Therefore, the online tuning has better speed response regardless of the drive cycle type. The speed overshoots are due to the overshoots and undershoots in the motor torque, as shown in Figs 10 and 11. Tables 4 and 5 summarize the difference between the offline and online tuning for the PI controller in the EV drive system under consideration for both drive cycles. It can be concluded from these tables that the utilization of the MLP-ANN online in the drive system, tested by the two drive cycles, provides lower values of MSE, IAE, and percentage overshoot in the motor speed compared with the offline tuning using TSO, i.e., better response.

The motor currents for the two drive cycles under consideration are shown in Figs 12 and 13. It can be noticed that the motor currents are almost sinusoidal. The total harmonic distortions (THDs) of the motor currents are shown in Figs 14 and 15 for the two drive cycles. It can be noticed from these figures that the THDs are slightly lower when the online running is used compared with the offline tuning.

Figs 16 and 17 show the required EV consumed energy and the actual energy consumed when offline and online tuning are used for the two driving cycles. It is clear from these figures that the energy consumed for online tuning using MLP-ANN is less than that of offline tuning using TSO. This is also shown in detail in Table 6. Consequently, the use of the MLP-ANN online tuning for the PI controller in the EVDS under consideration results in energy saving. It should be noticed that these energy savings happened during small time intervals, 195s for the ECE-15 drive cycle and 240s for the IM240 drive cycle. Consequently, the quantity of energy saved will be greater for a longer time. This energy saving results in cost reduction of charging the batteries and increasing their lifetime.

The MLP-ANN online tuning gains of the PI controller for the two driving cycles under consideration are shown in Figs 18 and 19.

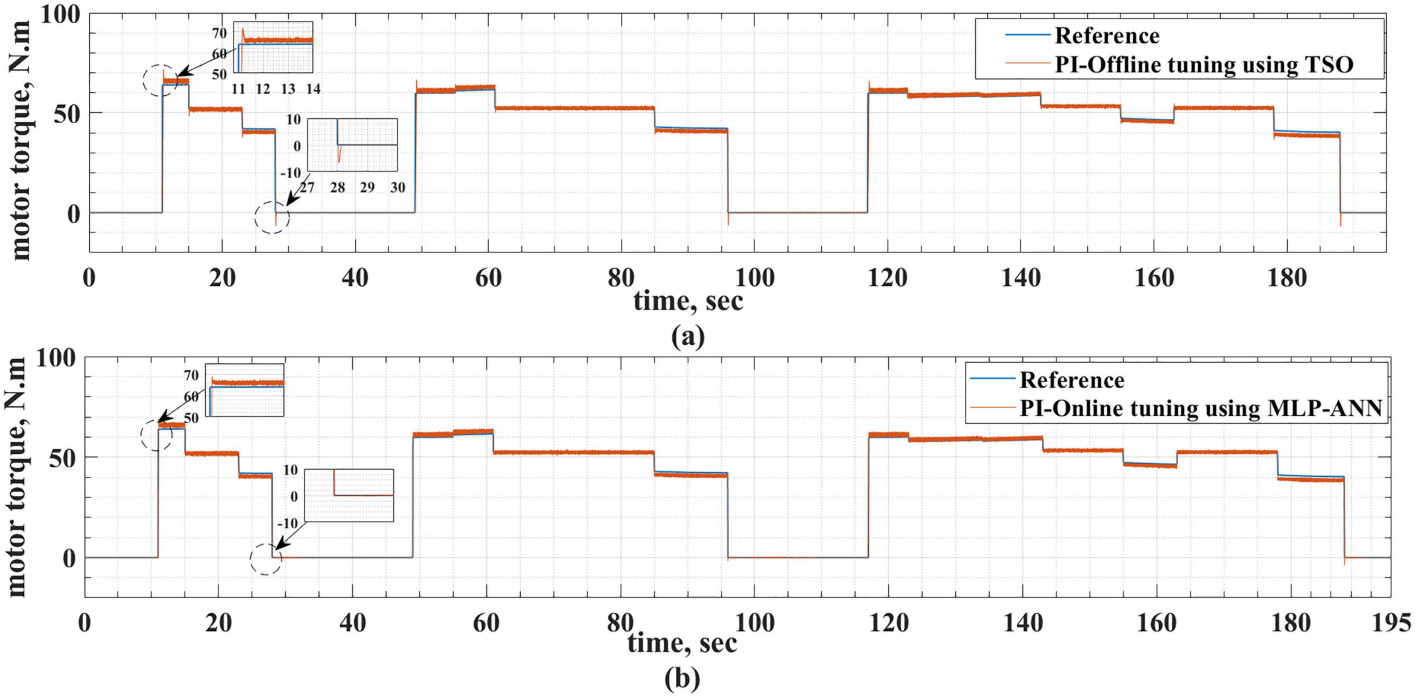

Fig 10. The reference and actual motor torque for the ECE-15 drive cycle when the offline and online PI tuning methods are used.

https://doi.org/10.1371/journal.pone.0340199.g010

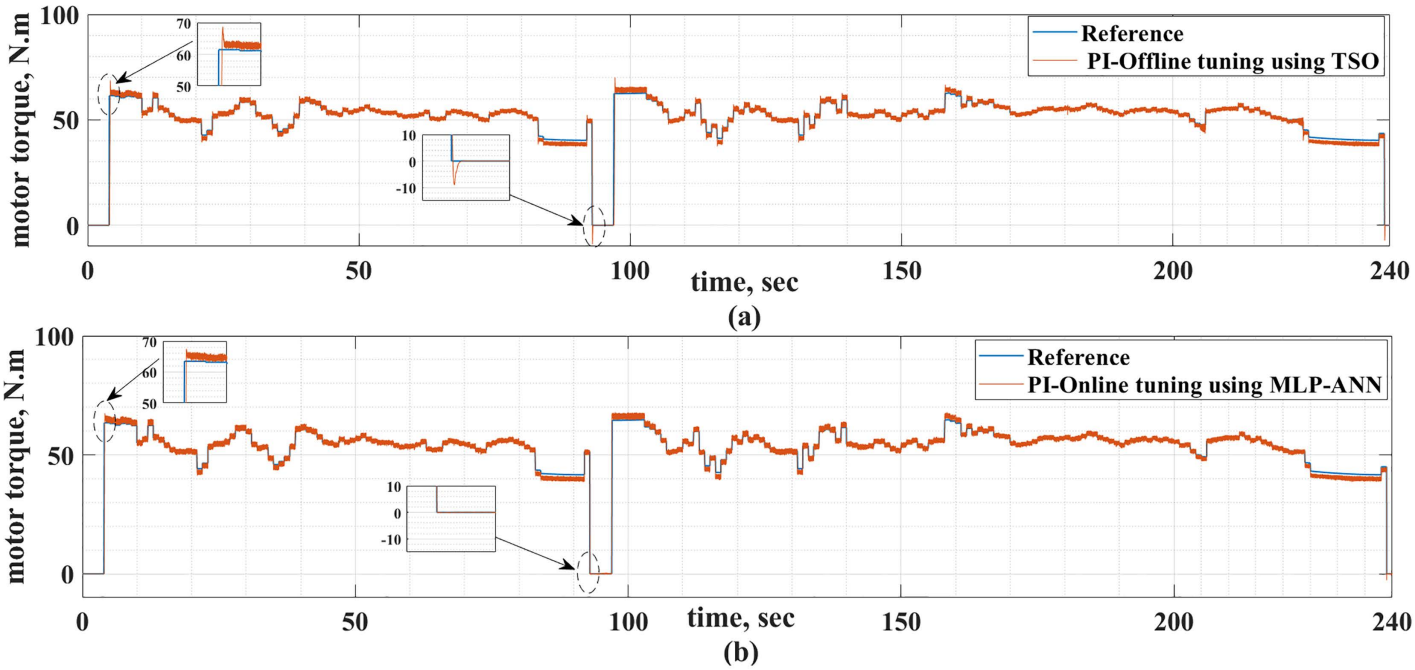

Fig 11. The reference and actual motor torque for the custom IM240 drive cycle when the offline and online PI tuning methods are used.

https://doi.org/10.1371/journal.pone.0340199.g011

Table 4. Speed response comparison between the PI-offline tuning using TSO and PI-online tuning using MLP-ANN when the ECE-15 drive cycle is used.

PI Tuning Method	MSE	IAE	Percentage Overshoot (%)
Offline tuning using TSO	0.009809	0.012091	1.658%
MLP-ANN online tuning	0.001737	0.002970	0.1366%

https://doi.org/10.1371/journal.pone.0340199.t004

Table 5. Speed response comparison between the PI-offline tuning using TSO and PI-online tuning using MLP-ANN when the custom IM240 drive cycle is used.

PI Tuning Method	MSE	IAE	Percentage Overshoot (%)
PI-offline tuning using TSO	0.007134	0.010105	3.334190%
PI-online tuning using MLP-ANN	0.001258	0.002529	0.006423%

https://doi.org/10.1371/journal.pone.0340199.t005

7 Conclusion

In this study, an efficient EV speed tracking control methodology is presented. This methodology is based on using an MLP-ANN online tuning for a PI controller. The adaptation of the five-phase IPMSM and MPC enhanced the efficiency and the reliability of the EV drive system. Two drive cycles, ECE-15 and custom IM240, are used to test the proposed control methodology of the EV drive system. A set of compared results between the offline tuning, using a recent metaheuristic optimization technique (TSO), and MLP-ANN online tuning for the PI controller used in the system under consideration. The result of the comparison showed that online tuning using MLP-ANN gives superior performance. The online tuning gives lower values of MSE, IAE, and percentage overshoot in the motor speed compared with the offline tuning method for the two test drive cycles adopted in this research. For the ECE-15 drive cycle, the MSE, IAE, and overshoot percentage are 0.001737, 0.002970, and 0.1366%, respectively, while for the IM240 drive cycle, the values are 0.001258,

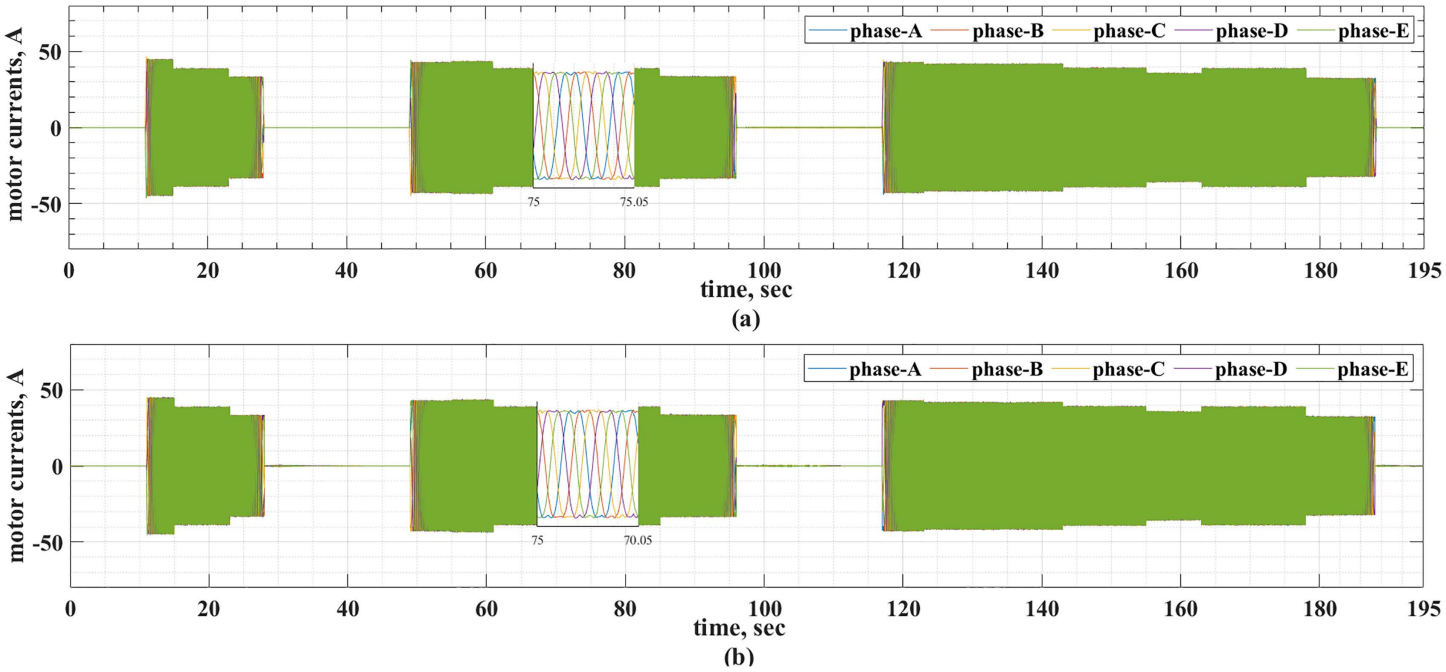

Fig 12. The motor currents for the ECE-15 drive cycles when (a) offline and (b) online PI tuning are used.

https://doi.org/10.1371/journal.pone.0340199.g012

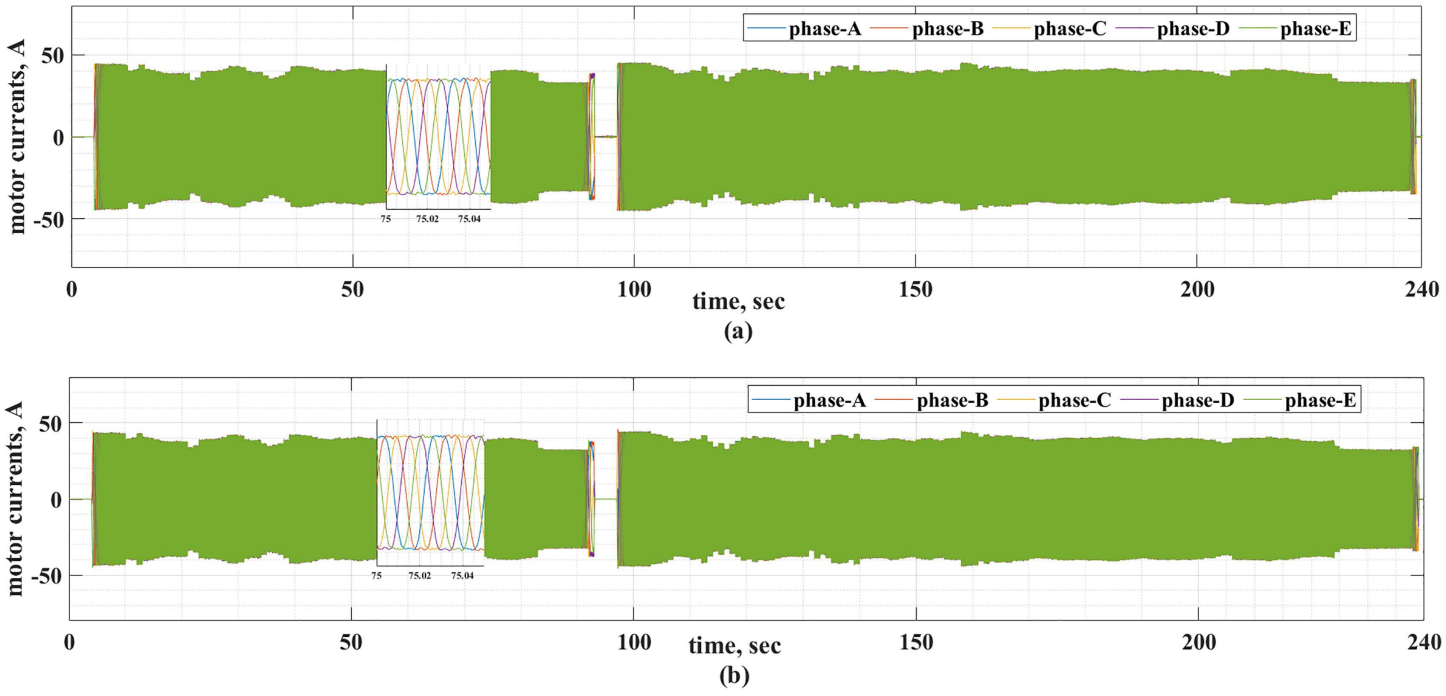

Fig 13. The motor currents for the custom IM240 drive cycle when (a) offline and (b) online PI tuning are used.

https://doi.org/10.1371/journal.pone.0340199.g013

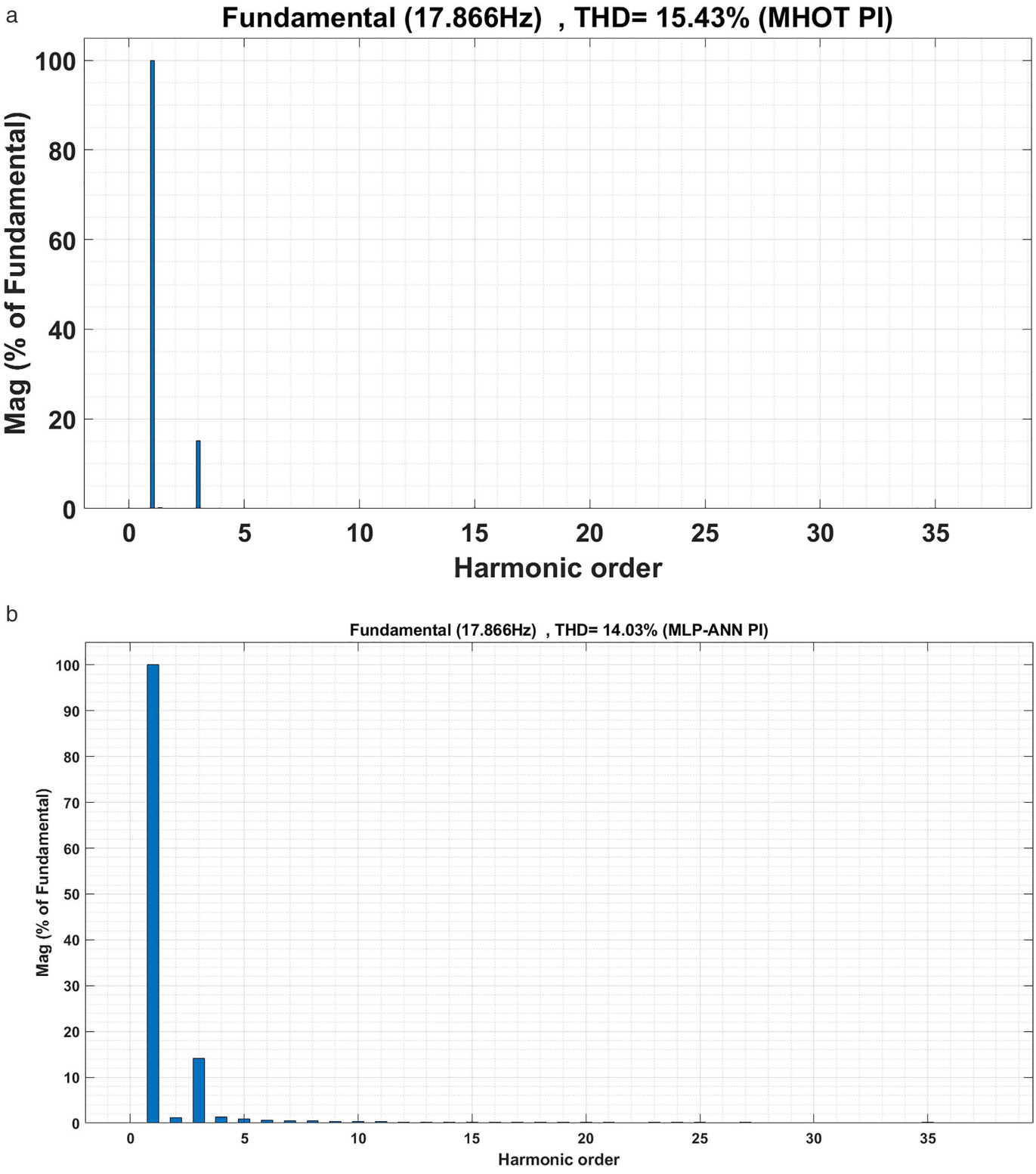

Fig 14. The motor currents THDs for the ECE-15 drive cycles when (a) offline and (b) online PI tuning are used.

https://doi.org/10.1371/journal.pone.0340199.g014

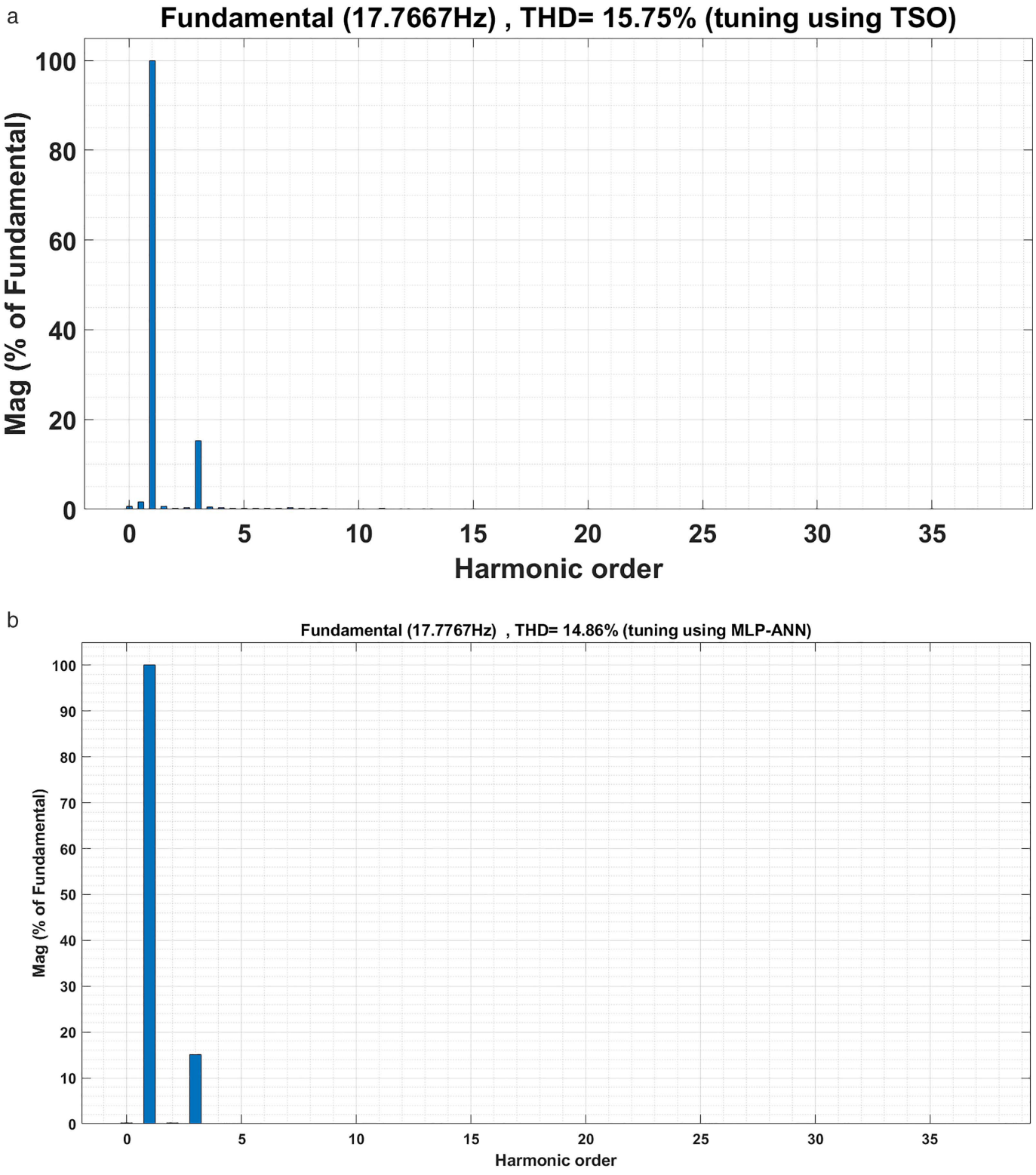

Fig 15. The motor currents THDs for the custom IM240 drive cycles when (a) offline and (b) online PI tuning are used.

https://doi.org/10.1371/journal.pone.0340199.g015

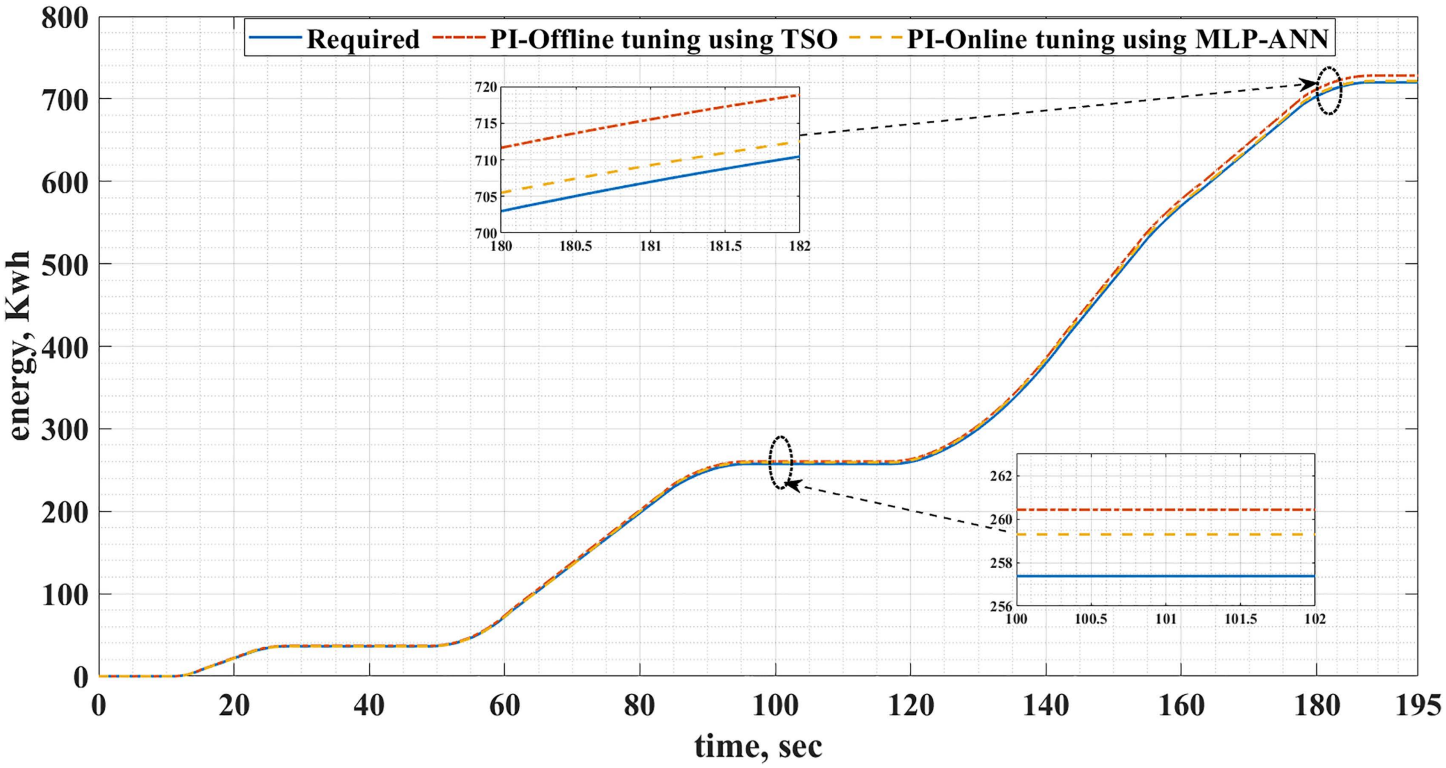

Fig 16. The required and actual EV energy consumed for the ECE-15 drive cycles when offline and online PI tuning are used.

https://doi.org/10.1371/journal.pone.0340199.g016

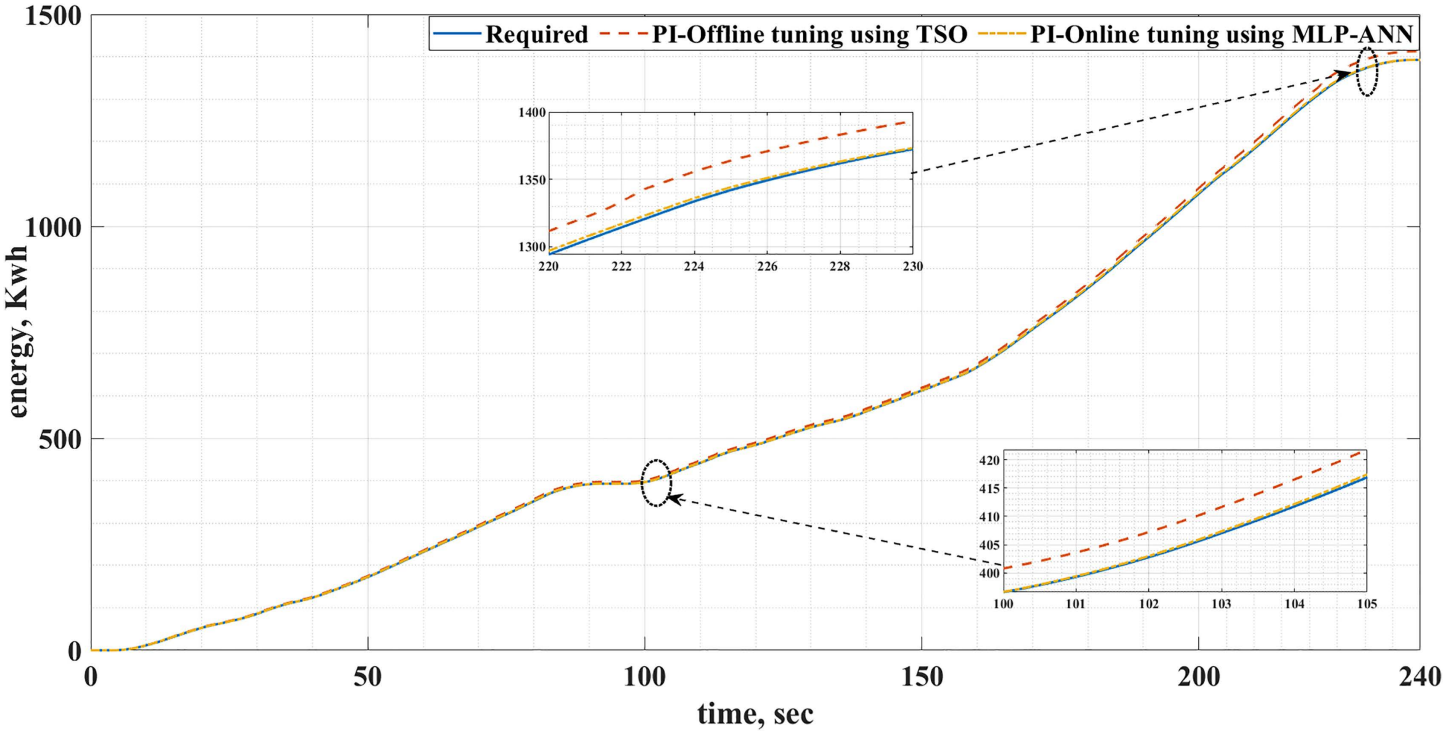

Fig 17. The required and actual EV energy consumed for the custom IM240 drive cycles when offline and online PI tuning are used.

https://doi.org/10.1371/journal.pone.0340199.g017

Table 6. Energy saving comparison between the offline and ANN online tuning for the two drive cycles.

Drive cycle	EV required Energy, kWh	Energy Consumption in case of Offline tuning using Transit Search, kWh	Energy Consumption in case of ANN online tuning, kWh	Energy Saving, kWh
ECE-15	719.984	732.458	728.074	4.39
Custom IM240	1392.592	1412.721	1392.582	20.13

https://doi.org/10.1371/journal.pone.0340199.t006

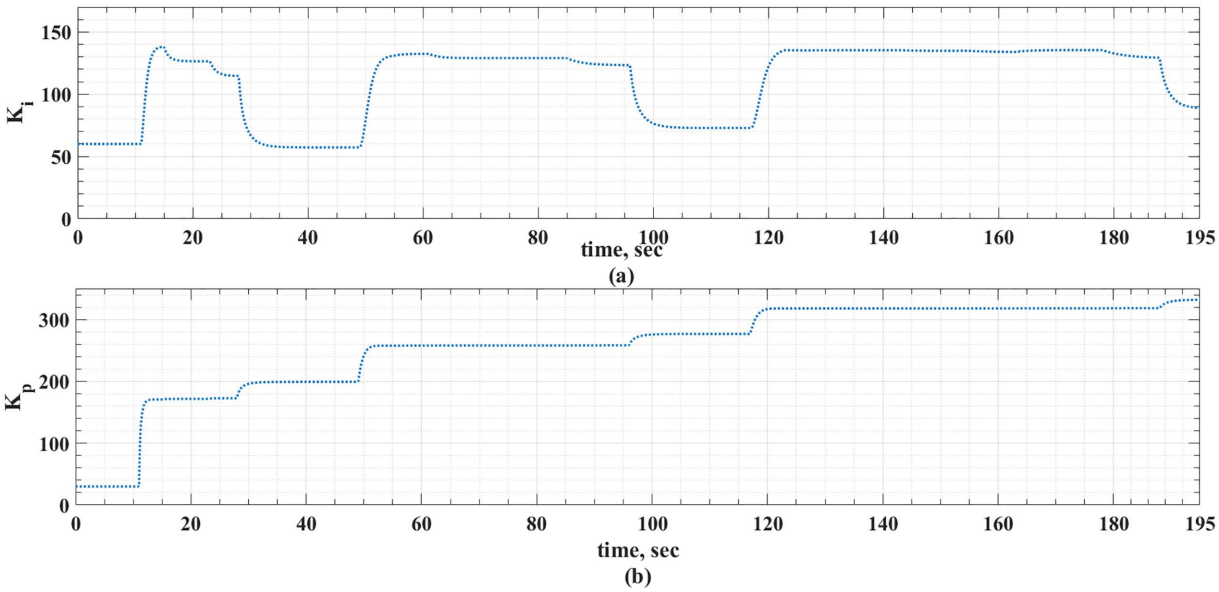

Fig 18. The PI-online tuning gains using MLP-ANN for the ECE-15 drive cycles.

https://doi.org/10.1371/journal.pone.0340199.g018

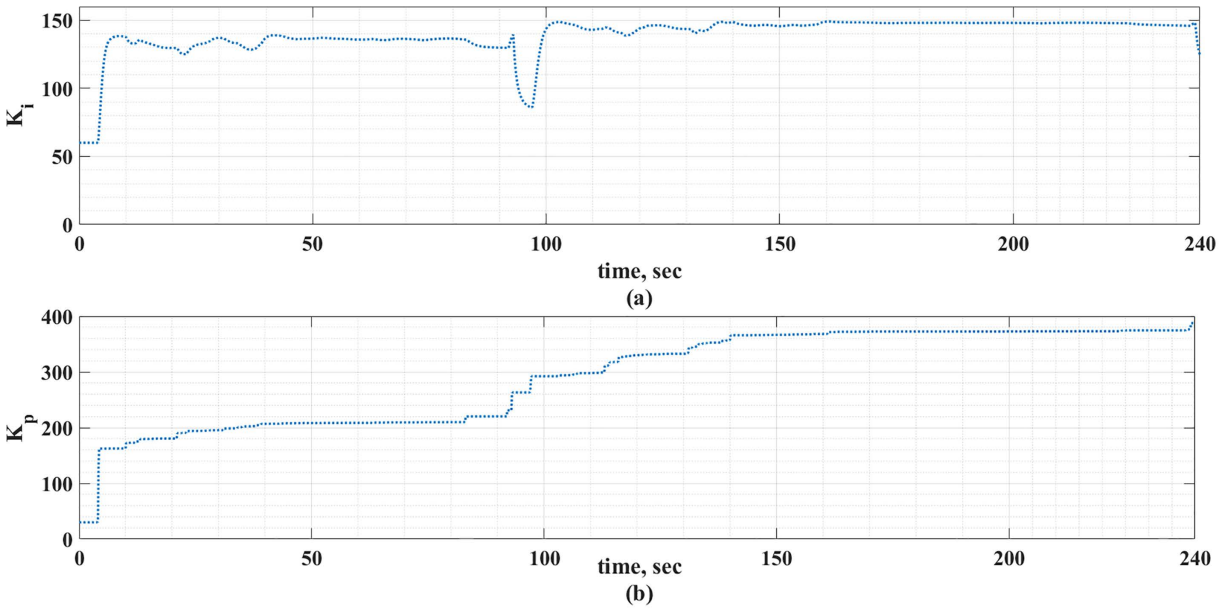

Fig 19. The PI-online tuning gains using MLP-ANN for the custom IM240 drive cycle.

https://doi.org/10.1371/journal.pone.0340199.g019

0.002529, and 0.006423%. Additionally, online tuning using MLP-ANN attains energy saving, with a maximum energy saving of 20.13 kWh compared to the conventional approach, which will be large over a long time, which in turn results in cost reduction of charging the batteries and increasing their lifetime. Finally, the THDs of the motor currents are slightly lower when the online tuning using MLP-ANN is used compared with the offline tuning using TSO. However, compared with offline tuning, online tuning has higher computational costs and potential delays in real-time applications. In addition to this, the implementation of online tuning algorithms is more complex.

Author contributions

Conceptualization: Ahmed M. Hassan, Mohamed Eladly Metwally.

Data curation: Mohammed M. Alammar.

Formal analysis: Hamada Esmaiel.

Investigation: Ahmed M. Hassan, Hamada Esmaiel, Mohammed M. Alammar, Mohamed Eladly Metwally.

Methodology: Ahmed M. Hassan.

Software: Hamada Esmaiel, Mohammed M. Alammar, Mohamed Eladly Metwally.

Validation: Hamada Esmaiel, Mohammed M. Alammar.

Writing – original draft: Ahmed M. Hassan, Hamada Esmaiel, Mohammed M. Alammar, Mohamed Eladly Metwally.

Writing – review & editing: Ahmed M. Hassan, Mohamed Eladly Metwally.

References

1. Lyu W, Hu Y, Liu J, Chen K, Liu P, Deng J, et al. Impact of battery electric vehicle usage on air quality in three Chinese first-tier cities. Sci Rep. 2024;14(1):21. https://doi.org/10.1038/s41598-023-50745-6 PMID: 38167600
2. Boumegouas MKB, Ilten E, Kouzi K, Demirtas M, M'hamed B. Application of a novel synergetic observer for PMSM in electrical vehicle. Electr Eng. 2024;106(5):5507–21. https://doi.org/10.1007/s00202-024-02297-9
3. Darwish A, Elgenedy MA, Williams BW. A review of modular electrical sub-systems of electric vehicles. Energies. 2024;17(14):3474. https://doi.org/10.3390/en17143474
4. Khanh PQ, Anh HPH. Hybrid optimal fuzzy Jaya technique for advanced PMSM driving control. Electr Eng. 2023;105(6):3629–46. https://doi.org/10.1007/s00202-023-01911-6
5. Mercorelli P. Control of Permanent Magnet Synchronous Motors for Track Applications. Electronics. 2023;12(15):3285. https://doi.org/10.3390/electronics12153285
6. Long L, Sun T, Liang J. Five phase permanent magnet synchronous motor decoupled model with dual frame frequency adaptive flux observer. Energy Reports. 2020;6:1403–8. https://doi.org/10.1016/j.egyr.2020.11.010
7. Tian B, Lu R, Hu J. Single Line/Phase Open Fault-Tolerant Decoupling Control of a Five-Phase Permanent Magnet Synchronous Motor under Different Stator Connections. Energies. 2022;15(9):3366. https://doi.org/10.3390/en15093366
8. Dharmasena S, Choi S. Model predictive control of five-phase permanent magnet assisted synchronous reluctance motor. In: 2019 IEEE Applied Power Electronics Conference and Exposition (APEC). 2019. 1885–90. https://doi.org/10.1109/apec.2019.8722267
9. Li J, Du B, Zhao T, Cheng Y, Cui S. Sensorless control of five-phase permanent-magnet synchronous motor based on third-harmonic space. IEEE Trans Ind Electron. 2022;69(8):7685–95. https://doi.org/10.1109/tie.2021.3111579
10. Cao B, Grainger BM, Wang X, Zou Y, Reed GF, Mao Z-H. Direct Torque model predictive control of a five-phase permanent magnet synchronous motor. IEEE Trans Power Electron. 2021;36(2):2346–60. https://doi.org/10.1109/tpel.2020.3011312
11. Zhao W, Wang H, Tao T, Xu D. Model predictive torque control of five-phase pmsm by using double virtual voltage vectors based on geometric principle. IEEE Trans Transp Electrific. 2021;7(4):2635–44. https://doi.org/10.1109/tte.2021.3063193
12. Bahar ST, Omar RG. Torque ripple alleviation of a five-phase permanent magnet synchronous motor using predictive torque control method. IJPEDS. 2022;13(4):2207. https://doi.org/10.11591/ijpeds.v13.i4.pp2207-2215
13. Huang W, Huang Y, Xu D. Model-free predictive current control of five-phase PMSM drives. Electronics. 2023;12(23):4848. https://doi.org/10.3390/electronics12234848
14. Rajanikanth P, Parvathy ML, Thippiripati VK. Enhanced Model predictive current control-based five-phase PMSM Drive. IEEE J Emerg Sel Topics Power Electron. 2024;12(1):838–48. https://doi.org/10.1109/jestpe.2023.3342653

15. Templos-Santos JL, Aguilar-Mejia O, Peralta-Sanchez E, Sosa-Cortez R. Parameter Tuning of PI Control for Speed Regulation of a PMSM using bio-inspired algorithms. Algorithms. 2019;12(3):54. https://doi.org/10.3390/a12030054
16. Raut AR, Jadhav SV. Model predictive speed control of permanent magnet synchronous motor. In: 2022 IEEE International Conference on Power Electronics, Drives and Energy Systems (PEDES). 2022. 1–6. https://doi.org/10.1109/pedes56012.2022.10080344
17. Li S, Won H, Fu X, Fairbank M, Wunsch DC, Alonso E. Neural-network vector controller for permanent-magnet synchronous motor drives: simulated and hardware-validated results. IEEE Trans Cybern. 2020;50(7):3218–30. https://doi.org/10.1109/TCYB.2019.2897653 PMID: 30802881
18. Liu H, Zhang H, Zhang H, Chen G. Model reference adaptive speed observer control of permanent magnet synchronous motor based on single neuron PID. J Phys: Conf Ser. 2022;2258(1):012052. https://doi.org/10.1088/1742-6596/2258/1/012052
19. Mao H, Tang X, Tang H. Speed control of PMSM based on neural network model predictive control. Transactions of the Institute of Measurement and Control. 2022;44(14):2781–94. https://doi.org/10.1177/01423312221086267
20. Nguyen TT, Tran HN, Nguyen TH, Jeon JW. Recurrent neural network-based robust adaptive model predictive speed control for pmsm with parameter mismatch. IEEE Trans Ind Electron. 2023;70(6):6219–28. https://doi.org/10.1109/tie.2022.3198255
21. Li H, Liu Z, Shao J. A Model predictive current control based on adaline neural network for PMSM. J Electr Eng Technol. 2022;18(2):953–60. https://doi.org/10.1007/s42835-022-01324-8
22. Wang B, Zhu J, Li Z, Li Y. An optimization algorithm used in PMSM model predictive control. IEICE Electron Express. 2024;21(2):20230444–20230444. https://doi.org/10.1587/elex.20.20230444
23. Song Z, Yang J, Mei X, Tao T, Xu M. Deep reinforcement learning for permanent magnet synchronous motor speed control systems. Neural Comput & Applic. 2020;33(10):5409–18. https://doi.org/10.1007/s00521-020-05352-1
24. Yeom K. Model predictive control and deep reinforcement learning based energy efficient eco-driving for battery electric vehicles. Energy Reports. 2022;8:34–42. https://doi.org/10.1016/j.egyr.2022.10.040
25. Nicola M, Nicola C-I. Improvement of linear and nonlinear control for pmsm using computational intelligence and reinforcement learning. Mathematics. 2022;10(24):4667. https://doi.org/10.3390/math10244667
26. Yin F, Yuan X, Ma Z, Xu X. Vector Control of PMSM Using TD3 Reinforcement Learning Algorithm. Algorithms. 2023;16(9):404. https://doi.org/10.3390/a16090404
27. Najem A, Moutabir A, Rafik M, Ouchatti A. Comparative Study of PMSM Control Using Reinforcement Learning and PID Control. In: 2023 3rd International Conference on Innovative Research in Applied Science, Engineering and Technology (IRASET). 2023. 1–5. https://doi.org/10.1109/iraset57153.2023.10153024
28. Harkat AR, Barazan L, Loukriz A, Bendib A. Improved control of permanent magnet synchronous motors using adaptive nonlinear control with Deadbeat Observer. SEES. 2024;5(1):2461–91. https://doi.org/10.54021/seesv5n1-122
29. Li H, Song B, Chen T, Xie Y, Zhou X. Adaptive fuzzy PI controller for permanent magnet synchronous motor drive based on predictive functional control. Journal of the Franklin Institute. 2021;358(15):7333–64. https://doi.org/10.1016/j.jfranklin.2021.07.024
30. Wang Y, Yu H, Niu S, Gu J, Liu Y, Cheng F, et al. Adaptive observer-based current constraint control for electric vehicle used PMSM. Applied Energy. 2024;360:122802. https://doi.org/10.1016/j.apenergy.2024.122802
31. Alpaslan E, Karaoğlan MU, Colpan CO. Investigation of drive cycle simulation performance for electric, hybrid, and fuel cell powertrains of a small-sized vehicle. International Journal of Hydrogen Energy. 2023;48(99):39497–513. https://doi.org/10.1016/j.ijhydene.2023.08.358
32. Jon R, Wang Z, Luo C, Jong M. Adaptive robust speed control based on recurrent elman neural network for sensorless PMSM servo drives. Neurocomputing. 2017;227:131–41. https://doi.org/10.1016/j.neucom.2016.09.095
33. George MA, Kamat DV, Kurian CP. Electric vehicle speed tracking control using an ANFIS-based fractional order PID controller. Journal of King Saud University - Engineering Sciences. 2024;36(4):256–64. https://doi.org/10.1016/j.jksues.2022.01.001
34. Kumar A, Chandekar A, Deshmukh PW, Ugale RT. Development of electric vehicle with permanent magnet synchronous motor and its analysis with drive cycles in MATLAB/Simulink. Materials Today: Proceedings. 2023;72:643–51. https://doi.org/10.1016/j.matpr.2022.08.304
35. Sangeetha E, Ramachandran VP. An enhanced proportional resonance controller design for the PMSM based electric vehicle drive system. Heliyon. 2024;10(15):e35244. https://doi.org/10.1016/j.heliyon.2024.e35244 PMID: 39166015
36. Sain C, Banerjee A, Biswas PK. Modelling and comparative dynamic analysis due to demagnetization of a torque controlled permanent magnet synchronous motor drive for energy-efficient electric vehicle. ISA Trans. 2020;97:384–400. https://doi.org/10.1016/j.isatra.2019.08.008 PMID: 31402045
37. Singirikonda S, Yeddula Pedda O. Investigation on performance evaluation of electric vehicle batteries under different drive cycles. Journal of Energy Storage. 2023;63:106966. https://doi.org/10.1016/j.est.2023.106966
38. Kasri A, Ouari K, Belkhier Y, Oubelaid A, Bajaj M, Berhanu Tuka M. Real-time and hardware in the loop validation of electric vehicle performance: Robust nonlinear predictive speed and currents control based on space vector modulation for PMSM. Results in Engineering. 2024;22:102223. https://doi.org/10.1016/j.rineng.2024.102223
39. Giang PT, Ha VT, Phuong VH. Drive Control of a Permanent Magnet Synchronous Motor Fed by a Multi-level Inverter for Electric Vehicle Application. Eng Technol Appl Sci Res. 2022;12(3):8658–66. https://doi.org/10.48084/etasr.4935

40. Tom AM, Febin Daya JL. Machine learning techniques for vector control of permanent magnet synchronous motor drives. Cogent Engineering. 2024;11(1). https://doi.org/10.1080/23311916.2024.2323813
41. Hassan AM, Ababneh J, Attar H, Shamseldin T, Abdelbaset A, Metwally ME. Reinforcement learning algorithm for improving speed response of a five-phase permanent magnet synchronous motor based model predictive control. PLoS One. 2025;20(1):e0316326. https://doi.org/10.1371/journal.pone.0316326 PMID: 39752401
42. Adeleke OP, Li Y, Chen Q, Zhou W, Xu X, Cui X. Torque Distribution Based on Dynamic Programming Algorithm for Four In-Wheel Motor Drive Electric Vehicle Considering Energy Efficiency Optimization. WEVJ. 2022;13(10):181. https://doi.org/10.3390/wevj13100181
43. Parsa L, Toliyat HA. Five-Phase Permanent-Magnet Motor Drives. IEEE Trans on Ind Applicat. 2005;41(1):30–7. https://doi.org/10.1109/tia.2004.841021
44. Parsa L, Kim N, Toliyat HA. Field Weakening Operation of High Torque Density Five-Phase Permanent Magnet Motor Drives. In: IEEE International Conference on Electric Machines and Drives, 2005., 2005. 1507–12. https://doi.org/10.1109/iemdc.2005.195920
45. Taşören AE, Gökçen A, Soydemïr MU, Şahïn S. Dikey Kalkış ve İniş Sistemi Modeli için Yapay Sinir Ağı Tabanlı Uyarlanır PID Kontrolör Tasarımı. European Journal of Science and Technology. 2020:87–93. https://doi.org/10.31590/ejosat.779085
46. Mirrashid M, Naderpour H. Transit search: An optimization algorithm based on exoplanet exploration. Results in Control and Optimization. 2022;7:100127. https://doi.org/10.1016/j.rico.2022.100127